

Photoelectron imaging of resonance-enhanced multiphoton ionization and above-threshold ionization of ammonia molecules in a strong 800-nm laser pulse

Le-Le Song(宋乐乐), Ya-Nan Sun(孙亚楠), Yan-Hui Wang(王艳辉), Xiao-Chun Wang(王晓春), Lan-Lai He(赫兰海), Si-Zuo Luo(罗嗣佐), Wen-Hui Hu(胡文惠), Qiu-Nan Tong(佟秋男), Da-Jun Ding(丁大军), Fu-Chun Liu(刘福春)

Citation: Chin. Phys. B . 2019, 28(6): 063201. **doi:** 10.1088/1674-1056/28/6/063201
Journal homepage: http://cpb.iphy.ac.cn; http://iopscience.iop.org/cpb

What follows is a list of articles you may be interested in

Photoelectron angular distributions of H ionization in low energy regime: Comparison between different potentials

Shu-Na Song(宋舒娜), Hao Liang(梁昊), Liang-You Peng(彭良友), Hong-Bing Jiang(蒋红兵)
Chin. Phys. B . 2016, 25(9): 093201. **doi:** 10.1088/1674-1056/25/9/093201

Field ionization process of Eu $4f^7 6snp$ Rydberg states

Zhang Jing, Shen Li, Dai Chang-Jian
Chin. Phys. B . 2015, 24(11): 113201. **doi:** 10.1088/1674-1056/24/11/113201

Lifetimes of Rydberg states of Eu atoms

Jing Hua, Ye Shi-Wei, Dai Chang-Jian
Chin. Phys. B . 2015, 24(1): 013203. **doi:** 10.1088/1674-1056/24/1/013203

Stark spectra of Rydberg states in atomic cesium in the vicinity of *n*=18

Dong Hui-Jie, Wang Ting, Li Chang-Yong, Zhao Jian-Ming, Zhang Lin-Jie
Chin. Phys. B . 2013, 22(7): 073201. **doi:** 10.1088/1674-1056/22/7/073201

Multiple-plateau structure and scaling relation in photoelectron spectra of high-order above-threshold ionization

Wu Yan,Ye Hui-Liang,Zhang Jing-Tao,Guo Dong-Sheng
Chin. Phys. B . 2012, 21(5): 053201. **doi:** 10.1088/1674-1056/21/5/053201

Photoelectron imaging of resonance-enhanced multiphoton ionization and above-threshold ionization of ammonia molecules in a strong 800-nm laser pulse*

Le-Le Song(宋乐乐)[1,2,3], Ya-Nan Sun(孙亚楠)[1,3], Yan-Hui Wang(王艳辉)[4], Xiao-Chun Wang(王晓春)[1,3], Lan-Hai He(赫兰海)[1,3], Si-Zuo Luo(罗嗣佐)[1,3], Wen-Hui Hu(胡文惠)[1,3], Qiu-Nan Tong(佟秋男)[1,3], Da-Jun Ding(丁大军)[1,3], and Fu-Chun Liu(刘福春)[1,3,†]

[1] *Institute of Atomic and Molecular Physics, Jilin University, Changchun* 130012, *China*
[2] *Jilin Institute of Chemical Technology, Changchun* 132022, *China*
[3] *Jilin Provincial Key Laboratory of Applied Atomic and Molecular Spectroscopy, Jilin University, Changchun* 130012, *China*
[4] *College of Electronic Science and Engineering, State Key Laboratory on Integrated Optoelectronics, Jilin University, Changchun* 130012, *China*

(Received 17 December 2018; revised manuscript received 2 April 2019; published online 8 May 2019)

In this work, we mainly investigate the NH_3 molecular multiphoton ionization process by using the photoelectron velocity map imaging technique. Under the condition of femtosecond laser (wavelength at 800 nm), the photoelectron images are detected. The channel switching and above-threshold ionization (ATI) effect are also confirmed. The kinetic energy spectrum (KES) and the photoelectron angular distributions (PADs) are obtained through the anti-Abel transformation from the original images, and then three ionization channels are confirmed successfully according to the Freeman resonance effect in a relatively low laser intensity region. In the excitation process, the intermediate resonance Rydberg states are $C^{\sim}{}^1A_1'$ ($6+2$ photons process), $B^{\sim}{}^1E''$ ($6+2$ photons process) and $C^{\sim}{}^1A_1'$ ($7+2$ photons process), respectively. At the same time, we also find that the photoelectron angular distributions are independent of laser intensity. In addition, the electrons produced by different processes interfere with each other and they can produce a spider-like structure. We also find ac-Stark movement according to the Stark-shift-induced resonance effect when the laser intensity is relatively high.

Keywords: photoelectron imaging, Rydberg state, resonance-enhanced multiphoton ionization, photoelectron angular distribution

PACS: 32.60.+I, 33.80.Rv, 33.60.+q **DOI:** 10.1088/1674-1056/28/6/063201

1. Introduction

In recent years, experiments based on photoelectron imaging and intense femtosecond laser have become a powerful tool to detect the evolution and internal structure of molecules. Ultra-fast dynamics have been widely investigated in molecular, atomic, and electronic systems in a strong laser field. Furthermore, science has always focused on the structural characteristics and dynamic characteristics of excited molecular states. By using the ultrafast laser-induced multiphoton ionization technique, we can study Rydberg states, continuous states, and lifetimes of the excited states, and we can also further understand the photoionization process. Keldysh found that the multi-photon absorption would result in above-threshold ionization (ATI) when the Keldysh parameter $\gamma > 1$.[1] The photoelectron energy spectrum is expressed as an equidistant peak structure with the energy difference being one photon's energy.[2–5] The high-resolution photoelectron spectrum measurement provides rich information about strong field ionization, such as the laser-induced electron diffraction,[6] resonance-like enhanced ionization,[7] and Freeman resonant ionization.[8,9] In the Freeman resonance region, the positions of peaks each are independent of laser intensity according to ponderomtotive potential. However, in the relatively high laser intensity region, it is similar to the plateau enhancement in atoms, the ac-Stark effect on high excited state (close to the ionization zone) or continuous state is different from the ac-Stark effect acting on the Freeman resonance region in ammonia molecules when the laser intensity is high enough. Based on the Stark-shift-induced resonance effects the position of photoelectron peak varies with the increase of the laser intensity and results in ac-Stark movement. The ac-Stark movement from ATI peak has been observed in many atomic systems, such as Ar[10] and Kr.[11]

Recently, strong field ionization of NH_3 molecules has become a popular topic.[12–16] The NH_3 is a typical oblate symmetric top. Because of the existence of orbital and vibrational degeneracies, the NH_3 molecule becomes an important system for studying the vibration interaction. In 1978, using $(2+2)$ REMPI technology, Colson *et al.*[17] studied the excited electronic states of NH_3 molecules, and discovered new electron states under the static pool[18] and molecular beam[19] conditions. At the same time, its rotation spectrum was also

*Project supported by the National Natural Science Foundation of China (Grant Nos. 11574116, 11534004, 10704028, and 11474123).
†Corresponding author. E-mail: lfc@jlu.edu.cn
© 2019 Chinese Physical Society and IOP Publishing Ltd

studied. Subsequently, in 1984, Ashfold and partners[20] further studied the spectrum of NH_3 molecules and high Rydberg states by using photoelectron spectroscopy and multiphoton ionization energy spectrum, which enriched our understanding of the structure of NH_3 molecules. In 1986, Xie *et al.*[21] detailed the $A^{\sim}\,{}^1A_2''$ state of NH_3 molecules by using ion dip spectroscopy, in which $(3+1)$ multiphoton ionization was used to study the NH_3 $C^{\sim'} \rightarrow X^{\sim}$ state spectrum. The structure and dynamics of NH_3 molecules were widely studied, especially its electronic states below the $C^{\sim'}\,{}^1A_1^{\sim}$ state. In 2000, Xie *et al.* investigated the predissociation information of NH_3 $A^{\sim}$ state through mass spectrometry and electron energy spectrum.[22]

Ionized electrons carry the initial atomic or molecular dynamics and structure information. Therefore, the analysis from the photoelectron angular distributions (PADs) and kinetic energy distributions (KEDs) can make us indirectly understand the molecular dynamics process and internal structure. From quantum controlled and state selected ammonia molecules, one can further investigate the NH_3 reaction dynamics and molecular dynamics.

2. Experiment

We studied the photoelectron imaging of NH_3 in an intense laser field. The experimental apparatus that was employed in the present work was described briefly and the details had been given in previous studies.[23,24] The laser system used in this work was a Ti:sapphire chirped-pulse amplification system with a central wavelength of 800 nm, which generated a pulse duration of 50 fs and a maximum value of 4-mJ output energy per pulse at a 1-kHz repetition rate. The laser intensity was calibrated by measuring the energy shift of the non-resonant ATI peaks of Xe; for further details, please see Refs. [25] and. [26] In our measurement, the laser polarization was parallel to the detector of velocity map imaging (VMI). The laser beams were focused on supersonic molecular beam through a convex lens. A neon carrier introduced 1% NH_3 into the source chamber via a 0.5-mm orifice of a pulsed valve (General Valve Series 9) at a repetition rate of 10 Hz. The molecular beam was produced and was then passed through a skimmer into the hexapole chamber where the rotational states were selected and focused by the inhomogeneous electrostatic field. Each rotational state selected molecular beam then crossed the laser at a right-angle in the interaction chamber. To obtain high-resolution images of electrons, the -5000 V/-3820 V voltage ratio was applied to the repeller and the extractor in the VMI. Two-dimensional photoelectron images were produced from the ionization of NH_3, and the signals were recorded by using a dual micro-channel plate/P47 phosphor screen in conjunction with a charge-coupled device (CCD) camera. All of the measurements were transferred into the computer for further processing.

3. Results and discussion

We investigate the resonance enhanced multiphoton ionization of ammonia in an 800-nm femtosecond intense laser system by using a VMI detector. The laser intensity ranges from 1.6×10^{13} W/cm^2 to 5.7×10^{13} W/cm^2. There are no other ion fragments in this experiment, which ensures that the electrons are ionized from the parent ions. The original images of two-dimensional velocity distributions are obtained by CCD.

To enhance the molecular beam intensity and the ionization signals, a hexapole is chosen. The force exerted on the molecules by the electric field governs the molecular motion inside the hexapole. The molecular trajectory follows the Newton differential equation

$$\frac{\mathrm{d}^2r}{\mathrm{d}t^2} = \frac{-1}{m}\frac{\mathrm{d}W}{\mathrm{d}E}\frac{\partial E}{\partial r}, \tag{1}$$

where $\partial E/\partial r$ is the electric field gradient, W is the energy including rotational energy W_{rot}, and W_{stark} is the Stark energy. One can readily determine the $\mathrm{d}W/\mathrm{d}E$ by using numerical or fitting method. The radial position is calculated by using the coupled partial derivative E as the molecule traverses the hexapole. The molecular trajectory motion is numerically calculated by using a fourth-order Runge–Kutta routine. The calculation method was detailed in our previous work.[27,28] In Fig. 1, the pure $|111\rangle$ state is extracted at a 3-kV focusing voltage. Almost pure $|222\rangle$ state is obtained at 7.8 kV, and the $|212\rangle$ state is obtained at 14 kV. To obtain a maximum single rotation state, we change the hexapole voltage to 7.8 kV. A signal increasing up to five times is achieved by selecting hexapole rotational states and focusing beams.

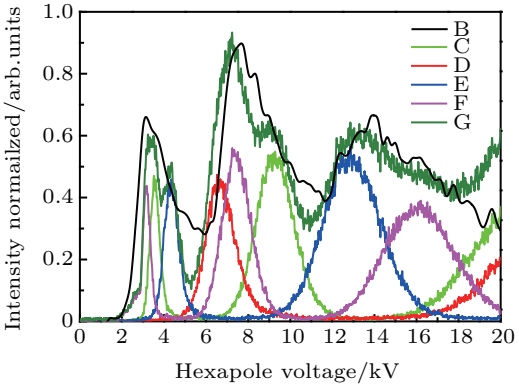


Fig. 1. NH_3 molecular hexapole focus curves. Curve B is for experimental results. Curves C, D, E, and F are for calculation results for $|111\rangle$, $|211\rangle$, $|212\rangle$, and $|222\rangle$ rotational states, respectively. Curve G is for sum of theoretical results.

The quantum controlled ammonia molecules interact with the 800-nm femetosecond laser behind the hexapole, and

the photoelectron images are detected. Figure 2 shows the ammonia photoelectron images. From Figs. 2(a)–2(e), we find the channel switching in low energy region from 1.6×10^{13} W/cm^2 to 2.7×10^{13} W/cm^2 (the inner ring is defined as channel 1 and the outer rings are defined as channels 2 and 3, respectively). When the laser intensity increases, the electronic population changes between channels 1, 2, and 3. When laser intensity continues to increase, as shown in Figs. 2(f)–2(j), higher-order ATI peaks are found, and the spider-like structures appear. This is because the tunneling ionization produces free electrons with high energy. The free electrons return to the parent ion under the action of oscillating laser field and fly out of the ionization region by the collision with the parent ion. The electrons produced by different processes interfere with each other, so it can produce spider-like structure.[29–32]

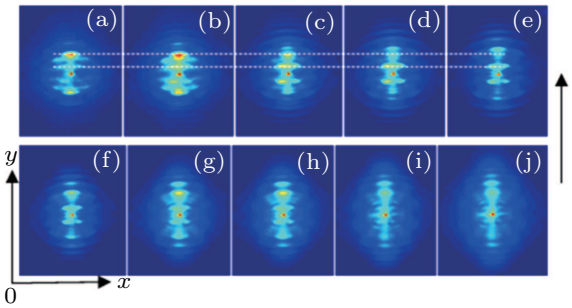


Fig. 2. NH_3 molecular photoelectron images at 800-nm laser wavelength. (a)–(e) Low laser intensity region. The laser intensities are 1.6×10^{13} W/cm^2, 1.9×10^{13} W/cm^2, 2.2×10^{13} W/cm^2, 2.5×10^{13} W/cm^2, and 2.7×10^{13} W/cm^2, respectively. (f)–(j) High laser intensity region. The laser intensities are 3.1×10^{13} W/cm^2, 3.8×10^{13} W/cm^2, 4.4×10^{13} W/cm^2, 5.0×10^{13} W/cm^2, and 5.7×10^{13} W/cm^2, respectively. Horizontal and vertical coordinates are x-pixel and y-pixel from CCD, and laser polarization direction is indicated by arrow.

To analyze the measurement results more directly and clearly, we extract the electron kinetic energy distributions from the original images. In Fig. 3, the horizontal axis represents electron kinetic energy. The single photon energy is 1.55 eV. We can find that the ATI peak 4 with a kinetic energy above 1.55 eV gradually moves to the left with increasing laser intensity. This is caused by the laser-induced above-threshold ionization, resulting in ac-Stark shift, which increases the ionization energy and reduces the remaining release energy. So peaks gradually move to the low energy positions. The structures of this region are more complex. After the energy continues to increase, the peak structure disappears. The region with energy less than 1.55 eV is the Freeman resonance region. From Fig. 3, only peak 3 clearly appears in the kinetic energy spectrum (KES) when the laser intensity equals 1.6×10^{13} W/cm^2. With the increase in laser intensity, peak 3 slowly decreases and peak 1 appears gradually, which is also consistent with what the original images show. The photoelectron population changes between peak 1, peak 2, and peak 3. The three peaks in the kinetic energy spectrum are 0.33 eV, 0.75 eV, and 0.99 eV, respectively. These peaks are involved in the multiphoton resonant absorption of some excited states, as generally seen in the case of atoms.[9,33,34]

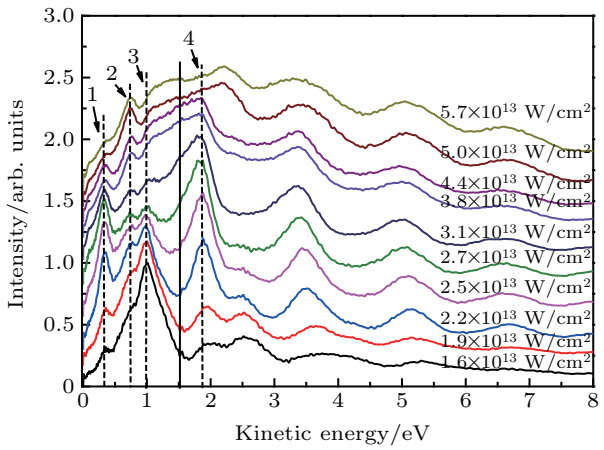


Fig. 3. Electron kinetic energy distributions of NH_3 molecules at 800 nm. Laser intensities are 1.6×10^{13} W/cm^2, 1.9×10^{13} W/cm^2, 2.2×10^{13} W/cm^2, 2.5×10^{13} W/cm^2, 2.7×10^{13} W/cm^2, 3.1×10^{13} W/cm^2, 3.8×10^{13} W/cm^2, 4.4×10^{13} W/cm^2, 5.0×10^{13} W/cm^2, 5.7×10^{13} W/cm^2. Numbers 1–4 represent peaks 1−4, respectively. Vertical solid black line refers to a single photon energy of 1.55 eV.

In the present experiment, the kinetic energy calibration is based on the electron imaging of the Xe atom, which is detected under the same condition. By converting the pixel points into kinetic energy and comparing with the corresponding Xe channels, we obtain the value of the kinetic energy calibration. The ATI peak shifts occur in the photoelectron energy spectrum, which is caused by changing laser intensity. According to the ponderomotive force potential, the up energy is in proportion to I/ω^2, ω is the laser frequency, and I is the laser intensity. Photoelectron energy distribution depends on relative laser intensity. The Xe photoelectron energy spectrum should satisfy $E_k = n\hbar\omega - (IP + U_p)$ where IP is the ionization potential, n is the number of photons absorbed in the process, and ω is the laser frequency. Based on above method, we obtain the relationship between U_p and I/ω^2, and we also obtain the relationship between laser intensity and laser pulse energy. The data processing of this experiment adopts Basex,[35] which is proposed by Vladimir and Dribinski *et al.*[35] Thus, the electron kinetic energy distributions are obtained and all signal strengths are normalized.

To find the intermediate states in Fig. 4, we show the energy shifts of various Rydberg states according to the U_p ($\sim I/\omega^2$) and $E'_R = E_R + U_p$, where E'_R is the Rydberg energy after considering the Stark shift in the laser field, and E_R is the Rydberg state energy without the laser field interaction (the E_R values of A, B, C, D, E Rydberg states are 5.73 eV, 7.34 eV, 7.92 eV, 8.65 eV, 9.04 eV, respectively). The 7.75 eV, 9.3 eV, and 10.85 eV horizontal lines are the values for five photons, six photons, and seven photons. In Fig. 4, we give the three

intermediate processes based on the three peaks in Fig. 3. For peak 3 in Fig. 3, the ammonia molecule absorbs six photons and resonates with the $C^{\sim}\,{}^1A_1'$ ($v=1$) state, then is excited to a continuous state ($v=0$) by absorbing two photons, and finally ionizes from the continuous state. The photoelectron kinetic energy is 0.99 eV, namely, the resonance enhanced multiphoton ionization (REMPI) process is (6+2). For peak 1 in Fig. 3, the ponderomotive force potential increases with the laser intensity (see Fig. 4), and six photons are not enough to make ammonia keep resonating with the $C^{\sim}\,{}^1A_1'$ state, but enough to make it resonate with the $B^{\sim}\,{}^1E'$ ($v=0$) state. The detected photoelectron kinetic energy is 0.33 eV. For peak 2 in Fig. 3, it absorbs seven photons to be resonant with the state $C^{\sim}\,{}^1A_1'$ ($v=0$) when the laser intensity continues to rise. It then continues to absorb two photons and ionizes from the continuous state ($v=1$), and the remanent photoelectron kinetic energy is 0.75 eV. From the energy analysis of Fig. 4, we find three multiphoton processes related to the three peaks in Fig. 3. The (6+2) process of the intermediate resonance state $C^{\sim}\,{}^1A_1'$ corresponds to the peak 3 in Fig. 3, the (6+2) process of state $B^{\sim}\,{}^1E''$ corresponds to peak 1 in Fig. 3, and the (7+2) process of state $C^{\sim}\,{}^1A_1'$ corresponds to peak 2 in Fig. 3.

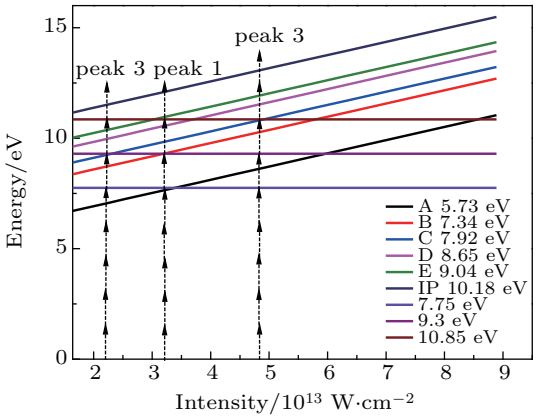


Fig. 4. Energy shifts of NH_3 molecular Rydberg states by adding ponderomotive force potential energy into the total energy. Without ponderomotive force, ionization potential of ammonia is 10.18 eV, and values of A, B, C, D, E states are 5.73 eV, 7.34 eV, 7.92 eV, 8.65 eV, 9.04 eV, respectively. The 7.75 eV, 9.3 eV, and 10.85 eV horizontal lines are values for 5 photons, 6 photons, and 7 photons.

To further identify our intermediate process, we extract the photoelectron angular distribution information from original images; as shown in Fig. 5. Generally, the angular distribution is represented by $I(\theta)$, where θ represents the angle between the direction of emission and the direction of laser polarization. Usually, $I(\theta)$ uses the Legendre polynomial fitting, and the expression is

$$I(\theta)=1+\sum a_L \mathrm{P}_L(\cos^2\theta)\quad (L=2,4,6), \tag{2}$$

where a_L are the Legendre polynomial coefficients.

From Fig. 5, we can see that the angular distributions from different peaks are also distinguishable. Here, we choose the laser polarization as 0° in the angular distribution. From Fig. 5, the photoelectrons of peak 1 are mainly located near 38° and 142°, and the number of the photoelectrons of peak 1 is close to 0 at 90°. The photoelectrons of peak 3 are located not only near 38° and 142°, but also around 90°. The photoelectrons of peak 2 are mainly located near 45° and 135°, but fewer around 90°. The photoelectron angular distribution has the same trend between peak 2 and peak 3. They are both from the intermediate $C^{\sim}\,{}^1A_1'$ state. The photoelectron angular distribution of peak 1 differs from the above two. This is because photoelectrons carry the information about the electron orbits. Therefore, the angular distribution is related to the molecular quantum number and the quantum number of angular momentum. At the same time, we find that peak 2 ($C^{\sim}\,{}^1A_1'$ state (7+2) process) is weaker than peak 3 ($C^{\sim}\,{}^1A_1'$ state (6+2) process). In other words, more photons lead to weaker peak. This proves the calibration of peak channels. We also compare the photoelectron angular distributions from the same peak at different laser intensities as shown in Fig. 6. Figures 6(a) and 6(b) represent the angular distributions of peaks 1 and 2, respectively. The angular distributions from the same peak almost do not change. This means that the photoelectron angular distribution on the same peak is independent of the laser intensity and is only related to its own electronic state.

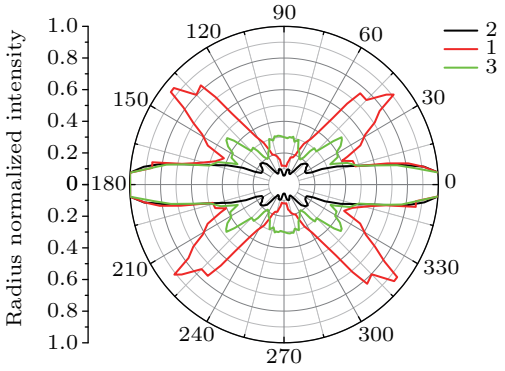


Fig. 5. Angular distributions of peak 1 $B^{\sim}$ state (6+2), peak 2 $C^{\sim}$ state (7+2), peak 3 $C^{\sim}$ state (6+2) in Fig. 4 according to Fig. 2. Red line is from peak 1, green line is from peak 3, and black line is from peak 2. The *r*-coordinate represents intensity/arb. unit.

With the combination of photoelectron kinetic energy distributions and photoelectron angular distributions, we identify each channel switching and intermediate process, as confirmed in Fig. 7. In the experiment, the Keldysh parameters of the molecules are mainly centered around $\gamma\approx 1$. Therefore, both multiphoton ionization and tunneling ionization will contribute to the measurement of photoelectron spectrum, which has been proven experimentally.[36,37] However, in this experiment, multiphoton ionization is a dominant factor. There might be some deviations in the results. First, the structure of NH_3 is complex and there are a lot of rotational states. This

makes it more difficult to identify the electronic states. Second, because the kinetic energy is calibrated according to the Stark effect of Xe, there are some deviations in the kinetic energy calibration. With the increase of laser intensity, the energy of vibrational state is closer to the ionization energy, so the energy levels do not produce the perfect Stark shifts.

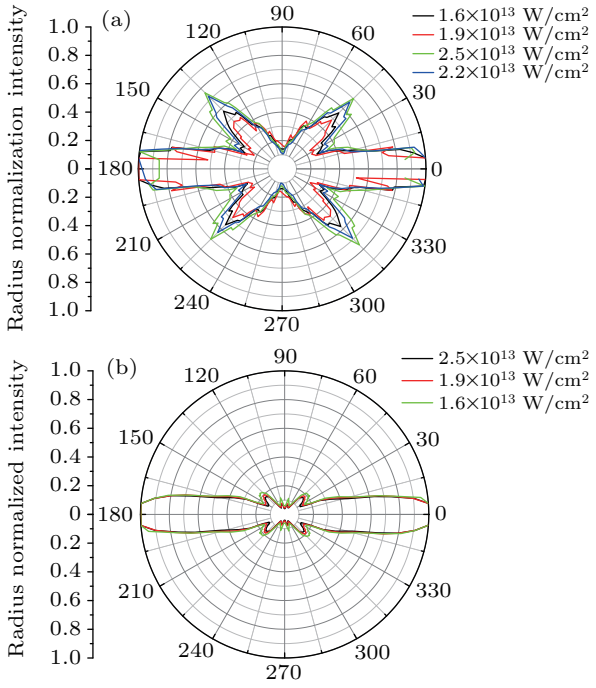


Fig. 6. Angular distributions of same peak with different laser intensities. Panel (a) is from peak 1 and panel (b) is from peak 2. The *r*-coordinate refers to intensity /arb.unit.

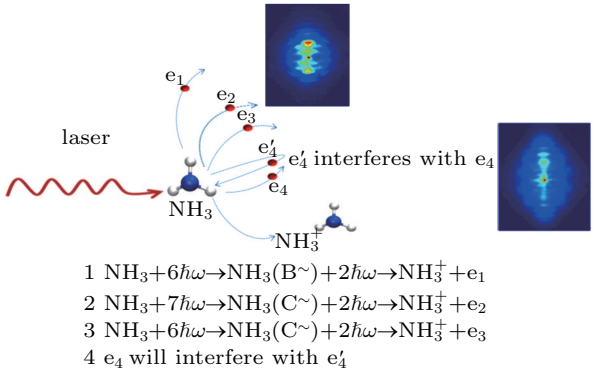


Fig. 7. Schematic illustration of NH_3 intermediate processes based on experimental results.

4. Conclusions

In this paper, we analyze the internal structure and resonance enhanced multiphoton ionization (REMPI) process of NH_3 molecules by using an 800-nm laser wavelength intense laser induced photoelectron velocity map imaging detection. First, the NH_3 molecular ionization is enhanced by hexapole. Then, the photoelectrons are focused by an ion lens in a velocity map imaging (VMI) system and they are collected by CCD to obtain the original images. The photoelectron velocity distributions and photoelectron angular distributions are extracted from the original images. Thus, the channel switching can be analyzed and we reveal the contribution of the resonance effect to the process of strong field ionization. By comparing the original photoelectron images and kinetic energy spectrum, the quantum state channel switching is confirmed. Combined with the identification of the literature and Freeman resonance technique, the results are analyzed and each peak is identified in the electron energy spectrum. We also show the possible causes and deviations. Under the condition of the 800 nm laser wavelength, photoelectron kinetic energy peaks are located at 0.99 eV, 0.33 eV, and 0.75 eV. In the excitation process, the intermediate resonance states are $C^{\sim}\ ^1A_1'$ $(6+2)$, $B^{\sim}\ ^1E''$ $(6+2)$, and $C^{\sim}\ ^1A_1'$ $(7+2)$ respectively. The peaks at less than 1.55 eV are the Freeman resonance results. We find that the angular distribution of each peak is distinguishable and photoelectron angular distributions from the same peak are independent of laser intensity. Meanwhile, when the peak energy is greater than 1.55 eV, the peak will move toward the left with laser intensity increasing. This happens because the Stark shift will increase the ionization energy. In addition, the overflow kinetic energy is larger than the energy of one photon, which is due to the occurrence of tunneling ionization. The electrons produced by different processes interfere with each other and can produce a spider-like structure. In this experiment, there is a certain deviation in photoelectron imaging due to various reasons. Therefore, it is necessary to improve the detection resolution and laser intensity calibration in future experiments. At least, through the present experimental measurement, the NH_3 channel switching is identified accurately. This will provide the key conditions for NH_3 reaction dynamics and molecular dynamics.

Acknowledgment

The authors thank Liu Fu-Chun's group for their helpful discussion.

References

[1] Guo L and Han S S 2012 *Phys. Rev. A* **86** 053409
[2] Li M, Liu Y, Liu H, Yang Y, Yuan J, Liu X, Deng Y, Wu C and Gong Q 2012 *Phys. Rev. A* **85** 13414
[3] Wiehle R, Witzel B, Helm H and Cormier E 2003 *Phys. Rev. A* **67** 063405
[4] Kumarappan V, Holmegaard L, Martiny C, Madsen C B, Kjeldsen T K, Viftrup S S, Madsen L B and Stapelfeldt H 2008 *Phys. Rev. Lett.* **100** 093006
[5] Becker W, Grasbon F, Kopold R, Milosevic D B, Paulus G G and Walther H 2002 *Adv. Atom. Mol. Opt. Phys.* **48** 35
[6] Ito Y, Wang C, Le A T, Okunishi M, Ding D, Lin C D and Ueda K 2016 *Struct. Dyn.* **3** 034303
[7] Wang C, Tian Y, Luo S, Roeterdink W G, Yang Y, Ding D, Okunishi M, Prümper G, Shimada K Ueda K and Zhu. R 2014 *Phys. Rev. A* **90** 023405
[8] Freeman R R, Bucksbaum P H, Milchberg H, Darack S, Schumacher D and Geusic M E 1987 *Phys. Rev. Lett.* **59** 1092

[9] Gibson G N, Freeman R R and Mcilrath T J 1992 *Phys. Rev. Lett.* **69** 1904
[10] Potvliege R M and Vucic S 2006 *Phys. Rev. A* **74** 023412
[11] Mevel E, Breger P, Trainham R, Petite G, Agostini P, Chambaret J P, Migus A and Antonetti A 1992 *J. Phys. B: At. Mol. Opt. Phys.* **25** L401
[12] Conaway W E, Morrison R J S and Zare R N 1985 *Chem. Phys. Lett.* **113** 429
[13] Urbanek J, Dahmen A, Torresalacan J, Königshoven P, Lindner J and Vöhringer P 2012 *J. Phys. Chem. B* **116** 2223
[14] Wells K L, Perriam G and Stavros V G 2009 *J. Chem. Phys.* **130** 074308
[15] Kang H, Dedonder-Lardeux C, Jouvet C, Grégoire G, Desfrançois C, Schermann J P, Barat M and Fayeton J A 2005 *J. Phys. Chem. A* **109** 2417
[16] Yu H, Evans N L, Chatterley A S, Roberts G M, Stavros V G and Ullrich S 2014 *J. Phys. Chem. A* **118** 9438
[17] Nieman G C and Colson S D 1978 *J. Chem. Phys.* **68** 5656
[18] Nieman G C and Colson S D 1979 *J. Chem. Phys.* **71** 571
[19] Glownia J H, Riley S J, Colson S D and Nieman G C 1980 *J. Chem. Phys.* **72** 5998
[20] Ashfold M N R, Bayley J M and Dixon R N 1984 *Chem. Phys.* **84** 35
[21] Xie J, Sha G, Zhang X and Zhang C 1986 *Chem. Phys. Lett.* **124** 99
[22] Xie J, Jiang B, Li G, Yang S, Xu J, Sha G, Xu D, Lou N and Zhang C 2000 *Faraday Discuss* **115** 127
[23] Dribinski V, Ossadtchi A, Mandelshtam V A and Reisler H 2002 *Rev. Sci. Instrum.* **73** 2634
[24] Luo S, Zhu R, He L, Hu W, Li X, Ma P, Wang C, Liu F, Roeterdink W G, Stolte S and Ding D 2015 *Phys. Rev. A* **91** 053408
[25] Hüter O and Temps F 2017 *Rev. Sci. Instrum.* **88** 046101
[26] Yu J, Hu W, Li X, Ma P, He L, Liu F, Wang C, Luo S and Ding D 2017 *J. Phys. B: At. Mol. Opt. Phys.* **50** 235602
[27] Liu F C, Jin M X, Gao X and Ding D J 2006 *Chin. Phys. Lett.* **23** 344
[28] Song L L, Wang Y H, Wang X C, Sun H T, He L H, Luo S Z, Hu W H, Li D X, Zhu W H, Sun Y N, Ding D J and Liu F C 2019 *Chin. Phys. B* **28** 023101
[29] Huismans Y, *et al.* 2011 *Science* **331** 61
[30] Hickstein D D, Ranitovic P, Witte S, Tong X M, Huismans Y, Arpin P, Zhou X, Keister K E, Hogle C W, Zhang B, Ding C, Johnsson P, Toshima N, Vrakking M J J, Murnane M M and Kapteyn H C 2012 *Phys. Rev. Lett.* **109** 073004
[31] Meckel M, Staudte A, Patchkovskii S, Villeneuve D, Corkum P, Dörner R and Spanner M 2014 *Nat. Phys.* **10** 594
[32] Arbó D G, Lemell C, Nagele S, Camus N, Fechner L, Krupp A, Pfeifer T, López S D, Moshammer R and Burgdörfer J 2015 *Phys. Rev. A* **92** 023402
[33] Li M, Zhang P, Luo S, Zhou Y, Zhang Q, Lan P and Lu P 2015 *Phys. Rev. A* **92** 063404
[34] Shao Y, Li M, Liu M M, Sun X, Xie X, Wang P, Deng Y, Wu C, Gong Q and Liu Y 2015 *Phys. Rev. A* **92** 013415
[35] Luo S, Hu W, Yu J, Zhu R, He L, Li X, Ma P, Wang C, Liu F and Roeterdink W G 2017 *J. Phys. Chem. A* **121** 777
[36] Gibson G, Luk T S and Rhodes C K 1990 *Phys. Rev. A* **41** 5049
[37] Rudenko A, Zrost K, Schröter C D, Jesus V L B D, Feuerstein B, Moshammer R and Ullrich J 2004 *J. Phys. B: At. Mol. Opt. Phys.* **37** L407